Excitation of Pseudorotational Vibronic Motion through Femtosecond Pump−Probe Spectroscopy: A 2D Computational Study

Jörg Schön and Horst Köppel*

Theoretische Chemie, Physikalisch−Chemisches Institut, Universität Heidelberg, INF 229, D-69120 Heidelberg, FRG

Received: May 14, 1999

The real-time excitation and detection of radial and pseudorotational vibronic motions of Jahn−Teller and pseudo-Jahn−Teller coupled systems is studied theoretically. A previously developed 2D description of ground and excited electronic states of the sodium trimer, Na_3, is employed as a realistic model system. Within this scheme the detection of vibronic motions proceeds by measuring the ion signal, possibly resolved for the kinetic energy of the ejected photoelectrons. It is demonstrated how by changing various pulse parameters, such as pulse length, strength, or carrier frequency, radial or pseudorotational motions in the ground or excited electronic states are selectively excited. The particularly interesting—and difficult—case of exciting the pseudorotational motion in the ground state manifold can be realized by using three different pulses.

I. Introduction

Femtosecond (fs) pump−probe spectroscopy, in its many different variants existing nowadays, has become a powerful tool to investigate fundamental photophysical and photochemical processes and the underlying interaction mechanisms.[1−4] One particular field where it has been successfully applied is the study of metal atom clusters where already for the smallest systems—alkali dimers and trimers—a wealth of information emerged (see, for example, refs 5−12). As regards the analysis of intramolecular interactions, for example, the usefulness of pump−probe spectroscopy for revealing the nuclear dynamics on conically intersecting potential energy surfaces has been demonstrated in theoretical work by Domcke and co-workers.[13]

Alkali atom trimers have been, and continue to be, of interest because of the nonrigidity of the nuclear framework and the associated highly fluxional nuclear motion, often extending over multiple minima of the potential energy surface. In addition, there are frequently many electronic states in a narrow energy range, rendering the usual adiabatic approximation questionable and leading to strong nonadiabatic coupling effects. In particular, there has been much attention in the literature on the case of a pseudorotational motion encircling a Jahn−Teller (JT) intersection of potential energy surfaces,[14−23] the latter being a special type of a conical intersection.[24−28] Here, even for low vibrational energies the singular behavior of the adiabatic electronic wave functions shows up as a corresponding sign change, or geometric phase, of the vibrational wavefunctions when encircling the locus of intersection in a closed loop.[25−32] Originally the B excited state of Na_3 was believed to be the first experimental example of a geometric phase in molecular spectroscopy,[16] but later this claim has been disproved.[20−22] From the theoretical side, a geometric phase is present in the X ground state of Na_3,[17,23,33] but the first experimental verification of this phase has been achieved recently in a lower excited (A) state of Na_3,[34] and similar evidence is emerging on the ground state of Li_3.[35]

It is the purpose of the present work to theoretically explore further aspects of nuclear motion on intersecting potential energy surfaces and their ramifications in femtosecond pump−probe spectroscopy. This work has already been started in ref 36 where the sensitivity of the time-resolved ionization signal to the presence/absence of the geometric phase in Na_3(B) was addressed. By comparing both companion calculations with the experimental spectra of Gerber et al.,[5,6] additional evidence against the geometric phase in Na_3(B) could be deduced. Now we extend these earlier calculations by varying the pulse parameters such as carrier frequency, duration, or intensity. In this way, we hope to achieve partial *control* over the type of motion (radial or pseudorotational) or the electronic state (ground or excited), excited by the laser and dominating the observable signal. Of particular interest here is a possible scenario of how to detect the geometric phase effect in pump−probe spectroscopy, for example, in the X ground state of Na_3 (for earlier work pursuing such a goal along somewhat different lines see ref 37). We mention that the importance of the pulse length for the selective excitation of the pseudorotational motion has been pointed out before in the literature.[12] The same holds for the possibility to excite ground state vibrational motion by strong laser pulses.[38−40] Because of the limitations of our computational model, described in section II, we cannot expect to get quantitative predictions for Na_3. Nevertheless, we believe that the trends of our results, presented in section III, will be of general interest for future work in the field. This point will be addressed once more in the concluding section IV.

II. Theory

A. The Hamiltonian. The molecular Hamiltonian used for this study is adopted from an earlier analysis of ground and excited electronic states of Na_3[20,21] augmented by the electronic ground state of Na_3^+.[36] As is well-known,[17,33] Na_3 in its electronic ground state (Na_3(X)) can be considered as JT distorted from the D_{3h} conformation to yield three equivalent $^2B_2$ minima and $^2A_1$ saddle points (in the appropriate C_{2v} point group). On the other hand, Na_3 in its B excited state (Na_3(B)) has been shown to be subject to strong pseudo-Jahn−Teller (PJT) interactions[17,20,21] between two nearly degenerate E and A electronic states leading also to a C_{2v} minimum energy conformation.[17] The earlier modeling rests on the use of a diabatic electronic basis in which the nuclear kinetic energy

10.1021/jp991565o CCC: $18.00
Published on Web 10/14/1999

becomes diagonal and the (off-diagonal) potential energy matrix is expanded in a Taylor series, up to second order in the nuclear displacements from the D_{3h} conformation. The totally symmetric vibrational coordinate is neglected in order to reduce the computational effort. Finally, the vibrational motion in the ground state of Na_3^+ which is not subject to vibronic interaction will be treated in the harmonic approximation.[36]

We denote the diabatic basis functions by $|\phi_{0\pm}\rangle$ for the Na_3 ground state, $|\phi_{1\pm}\rangle$ and $|\phi_{1A}\rangle$ for the excited state manifold, and $|\phi_2\rangle$ for the Na_3^+ ground state. The accompanying electron of Na_3^+ with energy E_k is represented by the ket $|k\rangle$, so that a complete basis function for $(Na_3^+ + e^-)$ is $|\phi_2\rangle|k\rangle \equiv |\phi_{2k}\rangle$. Together with the vibronic wave functions $|w_i(t)\rangle$, the time-dependent state vector reads

$$|\psi(t)\rangle = \sum_{=0\pm,1\pm,1A} |\phi_i\rangle|w_i(t)\rangle + \int_0^\infty |\phi_{2k}\rangle|w_{2k}(t)\rangle \, dE_k \quad (1)$$

and the time evolution of the system is given by Schrödinger's equation (with $\hbar \equiv 1$)

$$i\frac{\partial}{\partial t}|\psi(t)\rangle = H(t)|\psi(t)\rangle$$

The time-dependent Hamiltonian $H(t)$ consists of three contributions for the three states of the molecule/ion under consideration. The part for the ion includes also the accompanying electron. Within the approach outlined above $H(t)$ reads

$$H = H_{\text{Ground}} + H_{\text{Excited}} + H_{\text{Ion}} + H_{\text{Interact}} \quad (3)$$

$$H_{\text{Ground}} = \left[\hat{T}_N + \frac{\omega_0}{2}\rho^2\right](|\phi_{0+}\rangle\langle\phi_{0+}| + |\phi_{0-}\rangle\langle\phi_{0-}|) + |\phi_{0+}\rangle\left(k_0\rho e^{-i\phi} + \frac{g_0}{2}\rho^2 e^{2i\phi}\right)\langle\phi_{0-}| + \text{h.c.} \quad (4)$$

$$H_{\text{Excited}} = \left[\hat{T}_N + E_{1E} + \frac{\omega_1}{2}\rho^2\right](|\phi_{1+}\rangle\langle\phi_{1+}| + |\phi_{1-}\rangle\langle\phi_{1-}| + |\phi_{1A}\rangle\langle\phi_{1A}|) + |\phi_{1A}\rangle\left(l_1\rho e^{i\phi} + \frac{f_1}{2}\rho^2 e^{-2i\phi}\right)\langle\phi_{1-}| + |\phi_{1A}\rangle\left(l_1\rho e^{-i\phi} + \frac{f_1}{2}\rho^2 e^{2i\phi}\right)\langle\phi_{1+}| + \text{h.c.} \quad (5)$$

$$H_{\text{Ion}} = \int_0^\infty |\phi_{2k}\rangle\left[\hat{T}_N + E_2 + \frac{\omega_2}{2}\rho^2 + E_k\right]\langle\phi_{2k}| \, dE_k + \text{h.c.} \quad (6)$$

$$H_{\text{Interact}} = \vec{D}\cdot\vec{E}(t) + \text{h.c.} \quad (7)$$

$\hat{T}_N$ denotes the kinetic energy operator. The diagonal terms in eqs 4 and 5 represent the unperturbed motion in the E' ground state and $(E' + A_1')$ excited states of Na_3 as well as in the ground state of Na_3^+ with the harmonic frequencies $\omega_{0,1,2}$, respectively. E_{1E} stands for the energy of the E′ excited state in the D_{3h} conformation which is assumed[20] identical to that of the A_1' state; the corresponding ground state parameter is set to 0. E_2 is the energy minimum of the ionic potential surface. The (electronically) off-diagonal terms contain the various vibronic couplings. They depend on polar coordinates ρ and ϕ for the nuclear motion which are related to the dimensionless D_{3h} normal coordinates Q_x and Q_y by

$$\rho e^{i\phi} = Q_y + iQ_x \quad (8)$$

In the appropriate C_{2v} subgroup, Q_x corresponds to the normal coordinate of the bending mode, Q_y to that of the asymmetric stretching mode.[20,21,41] k_0 and g_0 are the linear and quadratic JT coupling constants for the ground state; the PJT couplings of the excited state are l_1 (linear) and f_1 (quadratic).

The interaction of the molecule with the radiation field, which is described classically, is treated in the dipole and rotating-wave approximation.[42,43] For weak field strengths this approximation is very good. The transition dipole elements in the *diabatic* basis are assumed not to depend on the nuclear coordinates (generalized Condon approximation) nor on the energy of the ionized electron. Choosing all transition dipole elements according to the symmetry of the involved states (E' and A'_1), we arrive at the following expression for the dipole operator:

$$\vec{D} = |\phi_{1-}\rangle\vec{\mu}_+^{\,\text{EE}}\langle\phi_{0+}| + |\phi_{1+}\rangle\vec{\mu}_-^{\,\text{EE}}\langle\phi_{0-}| + |\phi_{1A}\rangle\vec{\mu}_-^{\,\text{EA}}\langle\phi_{0+}| - |\phi_{1A}\rangle\vec{\mu}_+^{\,\text{EA}}\langle\phi_{0-}| + \int_0^\infty(|\phi_{2k}\rangle\vec{\mu}_-^{\,\text{I}}E_k\rangle\langle\phi_{1+}| - |\phi_{2k}\rangle\vec{\mu}_+^{\,\text{I}}(E_k)\langle\phi_{1-}|) \, dE_k \quad (9)$$

$$\vec{\mu}_\pm^{\,\text{X}} = \vec{\mu}_y^{\,\text{X}} \pm \vec{\mu}_x^{\,\text{X}}; \quad X = \text{EE, EA, I} \quad (10)$$

$\vec{\mu}_\pm^{\,\text{EE}}$ couples the ground and excited E' states, and $\vec{\mu}_\pm^{\,\text{EA}}$ similarly couples the ground E′ and the excited A_1' state. Due to the involved symmetries only the excited E′ system is coupled to $(Na_3^+ + e^-)$. The specific form of the dipole operator in eq 9 follows from group theoretical considerations, requiring that $\vec{D}$ forms the basis for an E′ irreducible representation in the D_{3h} point group. Lacking further knowledge about the μ's, we assume them to be real and of the same magnitude.

The electric field of the pulses has the following form:

$$\vec{E}(t) = \sum_{i=1}^{2}\vec{E}_i(t); \quad \vec{E}(t) = \vec{E}_{i0}\frac{e^{-i\Omega_i(t-t_{i0})}}{\sqrt{\sqrt{\pi}\sigma_i}}\exp\left[-\frac{(t-t_{i0})^2}{2\sigma_i^2}\right] \quad (11)$$

with the normalization

$$\int|\vec{E}_i(t)|^2 \, dt = |\vec{E}_{i0}|^2$$

The standard set of parameters, taken from ref 36 and used in the calculations below is collected in Table 1. This contains the parameters for the laser pulses as well as for the molecular Hamiltonian. The linear JT/PJT coupling constants are seen to amount to ∼4 vibrational quanta which corresponds to moderately strong coupling, in the usual nomenclature.[41] These parameters have been shown earlier to lead to a good 2D description of the TPI spectrum of $Na_3(B)$[36] (for a subsequent

TABLE 1: Parameters Used for Modeling the Pump−Probe Ionization Spectrum of Na_3

ω_0 (cm^{-1})	90.5
k_0	$5.35\omega_0$
g_0	$0.076\omega_0$
E_{1E} (cm^{-1})	15806
ω_1 (cm^{-1})	127
l_1	$3.07\omega_1$
f_1	$0.0045\omega_1$
E_2 (cm^{-1})	30658
$E_{\max}$ (cm^{-1})	508
ω_2 (cm^{-1})	102
$\vec{\mu}_\pm^{\,\text{EE}}\cdot\vec{E}_{10}$	$\mp 0.1\omega_1$
$\vec{\mu}_\pm^{\,\text{EA}}\cdot\vec{E}_{10}$	$0.1\omega_1$
$\vec{\mu}_\pm^{\,\text{I}}\cdot\vec{E}_{20}$	$\mp 0.2\omega_1$
$\sigma_i\sqrt{8\ln 2}$ (fs)	60
$\Omega_i/(2\pi c)$ (cm^{-1})	16051

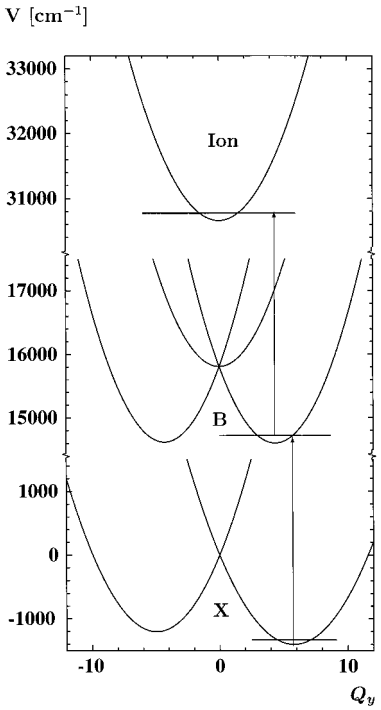

Figure 1. Potential energy curves for the parameter set of Table 1 representing various electronic states of Na_3.

3D description see ref 44). Cuts through the C_{2v} potential energy surfaces for these parameters, corresponding to $\varphi = 0$, $2\pi/3$, or $4\pi/3$ in eqs 4 and 5, are shown in Figure 1. For the underlying analytical expressions of these potential energy surfaces we refer to refs 20 and 21.

Computation of the Observable Signal. In the present calculations, the observable quantity is taken to be the (Na_3^+) ion yield as resulting from two femtosecond laser pulses that first excite the system from the ground (X) to the excited (B) state and second ionize the electronically excited molecule (see vertical arrows in Figure 1. The ionic signal, resolved for the energy of the accompanying electron, is

$$I(E_k,\Delta t) = \langle\psi(t\rightarrow\infty)|\phi_{2k}\rangle\langle\phi_{2k}|\psi(t\rightarrow\infty)\rangle = \langle w_{2k}(t\rightarrow\infty)|w_{2k}(t\rightarrow\infty)\rangle \quad (12)$$

with $\Delta t = t_{20} - t_{10}$, according to eq 11. Of particular interest here is the case of zero electron kinetic energy $E_k = 0$, leading to the time-resolved ZEKE spectrum (see, for example, refs 6, 13, and 45). The other relevant special case is the time-resolved total ion yield and is obtained simply as the integral of $I(E_k,\Delta t)$ over the whole kinetic energy range

$$I_{\text{total}}(\Delta t) = \int_0^\infty I(E_k,\Delta t)\, \mathrm{d}E_k \quad (13)$$

These observables are computed numerically[36] from the time-dependent wave function $\psi(t)$. The vibronic part of the latter is expanded in two-dimensional harmonic oscillator functions. For the numerical integration the complete Hamiltonian is again written as a sum $H_0 + H_I(t)$ of a time-independent part H_0 and an interaction part $H_I(t)$, the latter comprising all off-diagonal or vibronic coupling terms and the molecule−field interaction ($\vec{D}\cdot\vec{E}(t)$ + hc.). Since the dynamics of H_0 can be treated exactly, we transform eq 2 to the interaction picture and solve it numerically. The numerical integrator uses the Bulirsch−Stoer method (ref 46, Chapter 16) which we have found to be superior to other methods regarding accuracy and speed.

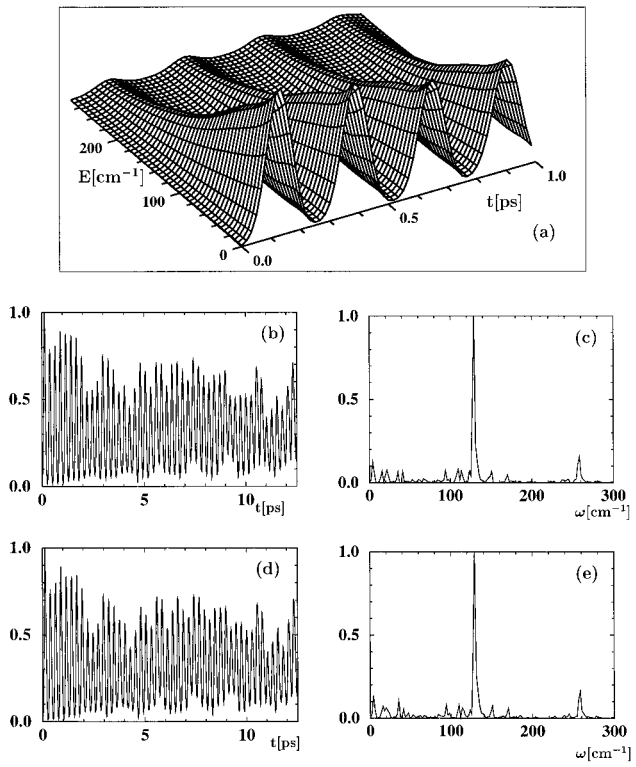

Figure 2. Results of pump−probe calculations on Na_3, using the parameter values from Table 1. The energy- and time-resolved ion signal is shown in (a), the total ion yield is shown in (b), and the Fourier spectrum of the latter in (c). In (d) and (e) we show ZEKE spectra with the same parameters.

For the discretization of the electron continuum we adopt the method of Burkey and Cantrell:[47,48] The electron continuum is included up to a maximum energy $E_{\max}$ and the energy dependence of $|w_{2k}(t)\rangle$ in the interval [0, $E_{\max}$] is expanded in terms of polynomials that are chosen orthogonal with respect to the transition dipole moment distributions $\vec{\mu}^{\,\mathrm{I}}_{\pm}(E)$. Taking $\vec{\mu}^{\mathrm{I}}_{\pm}(E)$ to be constant in the interval [0, $E_{\max}$] and 0 outside it, the polynomials in question are the Legendre polynomials.[47−49] It has been shown elsewhere[49] that this method produces good results even for a small number of expansion coefficients.

III. Results and Discussion

A. Excited State Dynamics. Figure 2 displays the results of our "reference" calculation with the standard set of parameters as listed in Table 1. Panels b and c are included for the ease of reading and reproduce Figure 2a of ref 36. The low-frequency structure of the Fourier-transformed ion signal (Figure 2b) has been taken in that earlier work as (additional) evidence for the PJT-dominated vibronic coupling mechanism in Na_3(B). The spectrum is dominated, however, in both the time and frequency domain, by the strong radial oscillation in the B-state with a frequency of $\approx$127 cm^{-1}. This is caused by the relatively small carrier frequencies of the pump and probe pulses of 16 051 cm^{-1} which were adopted from the experimental setup of refs 5 and 6. They allow for appreciable ionization only near the inner turning point of the B-state potential (see Figure 1). Therefore, the time-resolved photoelectron spectrum in Figure 2a always peaks at zero kinetic energy and the ZEKE spectrum displayed in panels d and e closely resembles the full ion signal from panels b and c. These findings already go beyond the results shown in ref 36 and are consistent with the experimental results of Baumert et al.[6] Together with the full time-resolved photo-

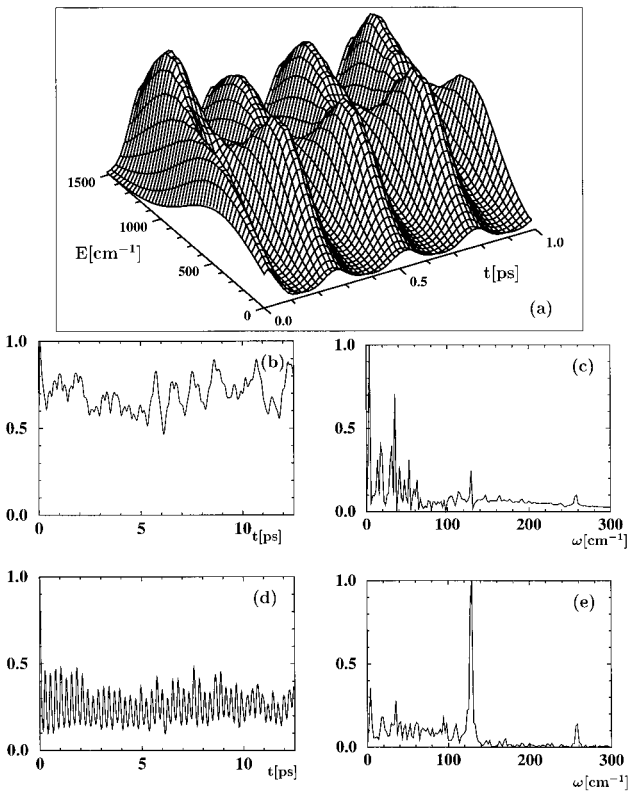

Figure 3. Same as Figure 2, but with the energy of the ionizing pulse being increased by 1613 cm^{-1}. The energy-resolved ion signal exhibits an oscillation with a period of 260 fs, as in Figure 2. This oscillation is still visible in the ZEKE spectrum, but due to the increased frequency of the second pulse it has almost no influence on the total ion yield.

electron spectrum in panel a they complete the analysis of the standard parameter set.

A modern issue in pump−probe spectroscopy is not only observation but also *control* of molecular dynamics. As regards Na_3 (B), the importance of the pulse length has been pointed out in the literature[12] which allows to selectively excite either pseudorotational or stretching motions. Here we wish to demonstrate that also the pulse wavelength is a suitable control parameter for that purpose. Figure 3 collects results for a situation completely analogous to Figure 2 but with the pulse carrier frequency being increased by 1613 cm^{-1}. This frequency is now large enough to allow for ionization at *all* values of ρ ($\equiv Q_y$ in Figure 1) which are relevant after excitation with the pump pulse. The mean photoelectron kinetic energy is still seen to oscillate in Figure 3a. However, the maximum of the kinetic energy distribution is now seen to occur at a nonzero value for all times. Hence the ZEKE signal (panels d and e) is seen to differ greatly from the full ion signal (panels b and c). Since the ZEKE signal mimics the oscillations of the electron kinetic energy, it is still dominated by the radial oscillations as in Figure 2, d and e. This, however, does not hold any more for the full ion yield which is seen to exhibit a rather irregular pattern with a much longer mean period than before. In fact, these are of the order of a picosecond as is the time scale of the pseudorotational motion.[7,12] In an intermediate frequency regime the pseudorotation can indeed affect the ion signal because the "radial" potential is a function of the pseudorotation angle (compare $Q_y \geq 0$ in Figure 1 which are not identical and represent $\phi = 0$ and π, respectively). Therefore, we attribute the time dependencies in Figure 3b as due to the pseudorotational motion. Of course, the present modeling is too simplified to allow for a quantitative prediction for Na_3 since higher order

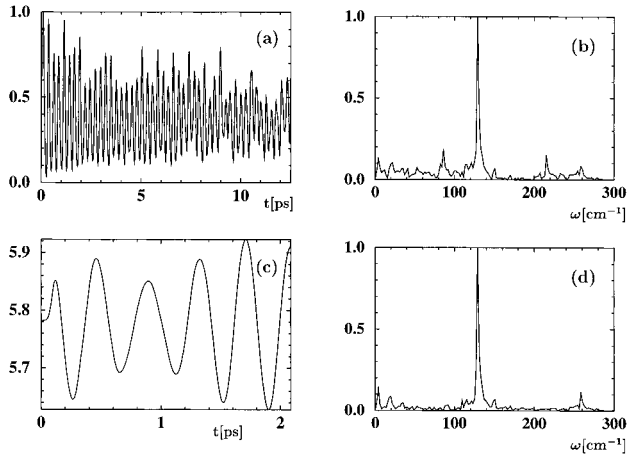

Figure 4. Detecting ground state dynamics in a pump−probe signal with increased laser pulse intensity. We show the signal and its Fourier transform in (a) and (b). To prove that the observed line at 86 cm^{-1} is due to the ground state dynamics, we show the mean value of the radial coordinate ρ in the ground state in (c) and a comparison calculation with disabling the probe−pulse coupling between ground and excited state in (d).

anharmonic terms, the Q-dependence of the transition matrix elements, and also the breathing mode are neglected. Nevertheless, we are convinced that the effect in question is in principle described correctly by our simulations. Therefore, they show another possible route to achieve selective excitation and detection of the pseudorotational over the radial motion.

B. Ground State Dynamics. So far, the pulse intensities considered were relatively weak and did not allow for excitation of ground state vibrational dynamics; rather the pump−probe sequence consisted of two one-photon transitions with the first photon exciting the system to the intermediate, or B, state and the second photon ionizing out of the latter. In Figure 4 we present results of a simulation with much stronger pulses, namely a pulse strength of 0.3ω for the pump pulse and 1.5ω for the probe pulse (in the earlier figures the pulse strengths are 0.1ω and 0.2ω, respectively; see Table 1, which still applies for all other parameters). The time-dependent signal resembles that in Figure 2, but the Fourier transform (FT) in Figure 4b shows an additional peak at $\approx$85 cm^{-1}. This corresponds to the frequency of the radial mode in the ground state (X state) potential energy surface; see Table 1. Indeed, there are significant radial oscillations in the X-state as computed from the expectation value $\langle\rho\rangle_X$ with the X-state component of the vibronic wave-packet (see Figure 4c). These arise from the first pulse pumping up to the B-state and then down again to the X-state, so that the relative displacement of the two potential surfaces leads to a coherent vibrational motion in the ground state. The second pulse finally ionizes out of the X-state. In a companion calculation the B−X coupling of the second pulse has been switched off and the peak at $\approx$85 cm^{-1} in the FT of the ion signal indeed disappears, as shown by Figure 4d.

The excitation of the ground state radial oscillation is clearly visible in Figure 4b but nevertheless relatively weak. Stronger excitation is possible, for example, with longer pump pulses. Figure 5 presents results with twice the pulse length of Figure 4, i.e., a pulse duration (fwhm) of 120 fs, but otherwise identical parameters. Now already the time-dependent signal in Figure 5a differs markedly from before, and its Fourier transform in Figure 5a is characterized by a strong (double) peak at $\approx$85 cm^{-1} which even exceeds the peak at $\approx$127 cm^{-1} in intensity. In other words, the ground state motion now dominates over the excited state motion in the total ion signal. Nevertheless,

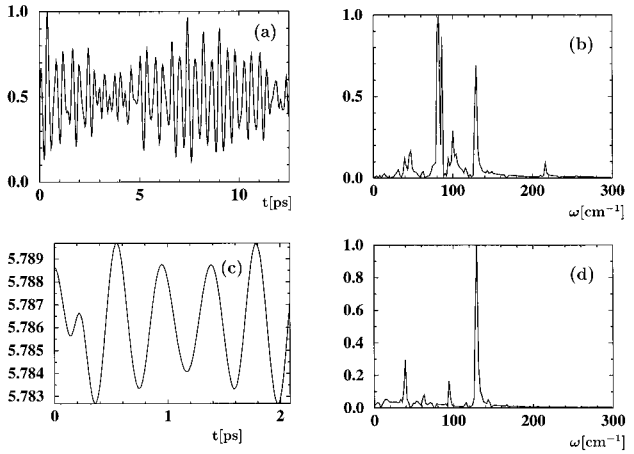

Figure 5. Influence of the pulse length on the observed ground state dynamics. We show the real time spectrum in (a), its Fourier transform in (b). Again as in Figure 4, we prove that the observed line at 86 cm^{-1} is due to ground state dynamics by showing the mean value of the radial coordinate ρ in (c) and a calculation with disabled probe−pulse coupling in (d).

the amplitude of the X-state radial oscillation is smaller than before; compare Figure 5c with Figure 4c. The stronger *relative* excitation in Figure 5b has to do with the smaller overall ionization probability in this situation. Companion calculations, not shown here in graphical form, reveal that the ion signal is reduced by about 2 orders of magnitude upon doubling the pulse length. This is a typical strong field effect and we attribute it to the well-known Rabi oscillations,[50,51] possibly also destructive interference of the two pathways of ionizing the systems (exciting to the B state only with the first or also with the second pulse). As a consequence, the absolute weakening of the radial oscillation in Figure 5c does not prevent it from dominating over the B-state motion in Figure 5b.

As stated in the Introduction, one of the main goals of this work is to show a possible route to identify the geometric phase in a time-resolved pump−probe experiment. Within our Na_3 (X,B) model system this amounts to selectively excite the X-state pseudorotational motion, thus combining the two effects addressed so far in the two subsections III A and III B. Not surprisingly, this goal proves quite difficult to accomplish. In fact, after a number of trial calculations it appears almost impossible to excite X-state pseudorotational motion with pump and probe pulses being of the form of eq 11 with the same constant carrier frequencies Ω_i ($i = 1, 2$). (The case of chirped pulses is discussed briefly below.) The reason is simple to understand from the characteristics of the X-state potential energy surface.[17,20,21] It consists of three equivalent minima being separated by saddle points with a barrier height of ∼180 cm^{-1}. Two pulses with the same wavelength almost invariably pump the system back to a location close to one of the minima where the pseudorotation amounts to a tunneling motion and is much too slow to be monitored with time delays available for femtosecond pulses (the tunneling splitting, according to ref 34, amounts to only ∼0.01 cm^{-1}).

In order to achieve a sensible excitation of X-state pseudorotation the second pulse should be red-shifted and thus place the system at an energy near that of one of the saddle points of the X-state potential. This is illustrated by Figure 6 which shows the results of a wavepacket propagation with an initial state located at one of these saddle points. The latter is displayed, together with a contour line drawing of the potential surface, in panel a. The subsequent panels nicely show the broadening of the wavepacket until it finally spreads completely around

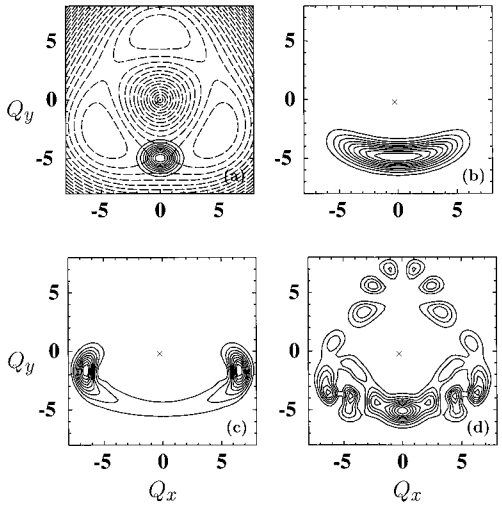

Figure 6. Ground state dynamics for a wave packet with initial position $Q_x = 0$, $Q_y = -5$, i.e., localized on a saddle point of the potential energy surface. We show times $t = 0$ fs in (a), $t = 167$ fs in (b), $t = 334$ fs in (c), and $t = 1$ ps in (d). Contour lines for the wavepacket are indicated as full lines, those for the potential energy surface are added in panel (a) as dashed lines.

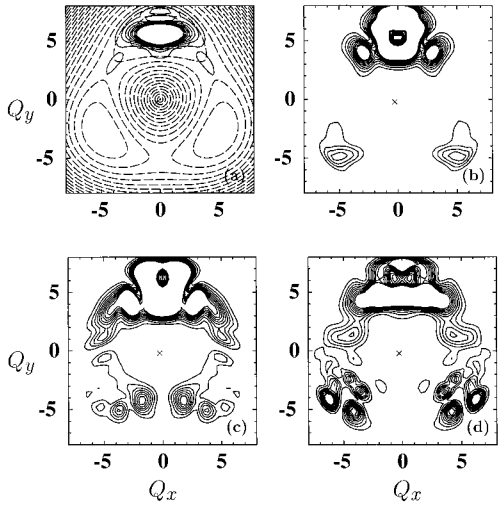

Figure 7. Ground state propagation after exciting with two pulses with frequencies 16 135.4 and 16 038.8 cm^{-1}. The time delay between the pulses is 245 fs. We show the ground state packet at times $T = 225$ fs in (a), $T = 475$ fs in (b), $T = 663$ fs in (c), and $T = 1.23$ ps in (d). For the meaning of the contour lines see Figure 6. To highlight the dynamics, the contour lines for the wavepacket only cover up to 25% of the maximum probability density in the ground state.

the JT conical intersection at the origin. In the upper half plane the line $Q_x = 0$ constitutes a nodal line where the wavefunction is locally *antisymmetric* under the mirror operation $Q_x \rightarrow -Q_x$. This is *opposite* to the behavior in the lower half-plane and represents the quantum dynamical manifestation of the geometric phase.[31,32,52,53] Note that the contour lines in Figure 6 represent the probability densities $|\psi(t)|^2$ and therefore do not reflect the symmetry properties directly. However, $|\psi(t)|^2$ is still seen to vanish along the upper half Q_y-axis, but is finite on the lower half Q_y-axis.

A complete revolution of the wavepacket around the X-state conical intersection is possible even without placing the system at one of the saddle points. Consider Figure 7 which displays the time evolution of a wavepacket after excitation with two realistic pulses of different wavelength. The first pulse is virtually the same as before and the second one is red shifted by ≈100 cm^{-1}. Both have the same pulse length (fwhm) of 60

fs. The time delay of 245 fs is chosen so that the wavepacket has reached the inner turning point of the radial oscillation when the second pulse has maximum intensity. At this time, also a substantial broadening along the pseudorotational angle has occurred in the excited state (see Figure 3 of ref 36). The red shift of the second pulse is chosen so as to be in resonance with the saddle point. Correspondingly, the wavepacket in panel a, at a time near the maximum of the second pulse (see figure caption), exhibits an appreciable pseudorotational broadening. Also, it is located energetically sufficiently highly above the minimum so that the pseudorotational motion proceeds on a fs time scale; see panels b and c. As soon as the wavepacket encircles the conical intersection at the origin, one recognizes the anomalous symmetry property in the lower and upper half-planes as described above. This is again a manifestation of the geometric phase which may be interpreted as arising from destructive interference of the different parts of the wavepacket encircling the conical intersection on opposite sides.[30,31] This behavior leads to a different *global shape* of the wavepacket and may be monitored with a third, ionizing pulse. As discussed in earlier work,[31,32,36] it will indeed show up in the corresponding time-dependent ion signal.

Finally, we repeat that the above investigation focused on the case of constant carrier frequencies of pump and probe pulses; see eq 11. The same goal might also be achieved by using a single chirped pulse, so that the molecule is pumped down by a suitable lower-frequency radiation at a later time during the pulse.

IV. Concluding Remarks

In this contribution we have explored possible routes to excite radial and pseudorotational motions in Jahn−Teller and pseudo-Jahn−Teller coupled systems by time-resolved pump−probe experiments, such as time-resolved ionization spectroscopy. The model system treated mimics important aspects of the X ground and B excited states of the sodium trimer. Thus, the ground state has been taken as a Jahn−Teller system and the excited state as a purely pseudo-Jahn−Teller coupled electronic manifold. Various possible routes to selectively excite either type of motion in the ground or excited electronic states have been indicated in this study. Also, the important issue of detecting the geometric phase in Na_3 (X) has been addressed above. (For another approach to detect geometric phase effects, by impulsive wavepacket interferometry, we refer to the work of J. Cina and co-workers.[37]) The present results cannot be considered a quantitative prediction for Na_3, due to the type of model adopted and the neglect of the breathing mode in the calculation. Nevertheless, important qualitative trends are not affected by this limitation. We mention the suppression of the radial motion in the excited state by increasing the carrier frequency of the pump pulse. This is caused by the PJT distortion in the excited state which is confirmed by ab initio calculations[17]. Also the existence of the geometric phase in Na_3(X) is well established from a theoretical point of view and its detection in real time would be highly desirable. Therefore, we hope that the present study may stimulate further experimental efforts in this interesting field.

Acknowledgment. The authors thank L. S. Cederbaum for his interest in this work. Financial support by the Deutsche Forschungsgemeinschaft is gratefully acknowledged.

References and Notes

(1) Zewail, A. H. *Femtochemistry*; World Scientific: Singapore, 1994; Vol. 1, 2.

(2) Zewail, A. H.; Bernstein, R. *The Chemical Bond*; Academic Press: New York, 1992.

(3) Zewail, A. H. *J. Phys. Chem.* **1993**, *97*, 12427.

(4) Manz, J.; Wöste, L. *Femtosecond Chemistry*; Verlag Chemie: Weinheim, Germany, 1995.

(5) Baumert, T.; Thalweiser, R.; Weiss, V.; Gerber, G. *Z. Phys. D.* **1993**, *26*, 131.

(6) Baumert, T.; Thalweiser, R.; Gerber, G. *Chem. Phys. Lett.* **1993**, *209*, 29.

(7) Gaus, J.; Kobe, K.; Bonačić-Koutecký, V.; Kühling, H.; Manz, J.; Reischl, B.; Rutz, S.; Schreiber, E. ;Wöste, L. *J. Phys. Chem.* **1993**, *97*, 12509.

(8) Meier, C.; Engel, V. *Phys. Rev. Lett.* **1994**, *73*, 3207.

(9) de Vivie-Riedle, R.; Reischel, B.; Rutz, S.; Schreiber, E. *J. Phys. Chem.* **1995**, *99*, 16829.

(10) Wolf, S., et al. *Phys. Rev. Lett.* **1995**, *74*, 4177.

(11) Ruppe, H.; Rutz, S.; Schreiber, E.; Wöste, L. *Chem. Phys. Lett.* **1996**, *257*, 356.

(12) Reischl, B.; de Vivie-Riedle, R.; Rutz, S.; Schreiber, E. *J. Chem. Phys.* **1996**, *104*, 8857.

(13) Domcke, W.; Stock, G. *Adv. Chem. Phys.* **1997**, *100*, 1.

(14) Gerber, W. H.; Schumacher, E. *J. Chem. Phys.* **1978**, *69*, 1692.

(15) Thompson, T. C.; Izmirlian, G.; Lemon, S. J.; Truhlar, D. G.; Mead, C. A. *J. Chem. Phys.* **1985**, *82*, 5597.

(16) Delacrétaz, G; Grant, E. R.; Whetten, R. L.; Wöste, L.; Zwanziger, J. W. *Phys. Rev. Lett.* **1986**, *56*, 2598.

(17) Cocchini, F.; Upton, T. H.; Andreoni, W. *J. Chem. Phys.* **1988**, *88*, 6068.

(18) Wolf, J. P.; Delacrétaz, G.; Wöste, L. *Phys. Rev. Lett.* **1989**, *63*, 1946.

(19) Dugourd, P.; Chevaleyre, J.; Perrot, J. P.; Broyer, M. *J. Chem. Phys.* **1990**, *93*, 2332.

(20) Meiswinkel, R.; Köppel, H. *Chem. Phys.* **1990**, *144*, 117.

(21) Meiswinkel, R.; Köppel, H. *Z. Phys. D* **1991**, *19*, 63.

(22) Ernst, W. E.; Rakowsky, S. *Phys. Rev. Lett.* **1995**, *74*, 58.

(23) Kendrick, B. *Phys. Rev. Lett.* **1997**, *79*, 2431.

(24) Carrington, J. *Acc. Chem. Res.* **1974**, *7*, 20.

(25) Longuet-Higgins, H. C. *Proc. R. Soc. London A* **1975**, *344*, 147.

(26) Köppel, H.; Domcke, W.; Cederbaum, L. S. *Adv. Chem. Phys.* **1984**, *57*, 59.

(27) Yarkony, D. R. *J. Phys. Chem.* **1996**, *100*, 18612.

(28) Yarkony, D. R. *Rev. Mod. Phys.* **1996**, *68*, 985.

(29) Berry, M. V. *Proc. R. Soc. London A* **1984**, *392*, 45.

(30) Mead, C. A. *Rev. Mod. Phys.* **1992**, *64*, 51.

(31) Schön, J.; Köppel, H. *J. Chem. Phys.* **1995**, *103*, 9292.

(32) Schön, J.; Köppel, H. *J. Chem. Phys.* **1998**, *108*, 1503.

(33) Martin, R. L.; Davidson, E. R. *Mol. Phys.* **1978**, *35*, 1713.

(34) von Busch, H.; Dev, V.; Eckel, H.-A.; Kasahara, S.; Wang, J.; Demtröder, W.; Sebald, P.; Meyer, W. *Phys. Rev. Lett.* **1998**, *81*, 4584.

(35) Keil, M.; Demtröder, W. private communication.

(36) Schön, J.; Köppel, H. *Chem. Phys. Lett.* **1994**, *231*, 55.

(37) Cina, J. A.; Smith, T. J., Jr.; Romero-Rochin, V. *Adv. Chem. Phys.* **1993**, *83*, 1.

(38) Hartke, B.; Kosloff, R.; Ruhmann, S. *Chem. Phys. Lett.* **1989**, *158*, 238.

(39) Baumert, T.; Meier, C.; Gerber, G.; Engel, V. *Chem. Phys. Lett.* **1992**, *200*, 488.

(40) de Vivie-Riedle, R.; Kobe, K.; Manz, J.; Meyer, W.; Reischl, B.; Rutz, S.; Schreiber, E.; Wöste, L. *J. Phys. Chem.* **1996**, *100*, 7789.

(41) Bersuker, I. B.; Polinger, V. Z. *Vibronic interactions in Molecules and Crystals*; Springer-Verlag: Berlin, 1989.

(42) Bloch, F.; Siegert, A. *Phys. Rev.* **1940**, *57*, 522.

(43) Silverman, M. P.; Pipkin, F. M. *J. Phys. B.* **1972**, *5*, 1844.

(44) Reischl, B. *Chem. Phys. Lett.* **1995**, *239*, 173.

(45) Müller-Dethlefs, K.; Schlag, E. W. *Annu. Rev. Phys. Chem.* **1991**, *42*, 109.

(46) Press, W. H.; Teukolsky, S. A.; Vetterling, W. T.; Flannery, B. P. *Numerical Recipes* in C, 2nd ed.; University Press: Cambridge, UK, 1992.

(47) Burkey, R. S.; Cantrell, C. D. *J. Opt. Soc. Am. B* **1984**, *1*, 169.

(48) Burkey, R. S.; Cantrell, C. D. *J. Opt. Soc. Am. B* **1985**, *2*, 451.

(49) Seel, M.; Domcke, W. *J. Chem. Phys.* **1991**, *95*, 7806.

(50) Cohen-Tannoudji, C.; Diu, B.; Laloë, F. *Quantum mechanics*; John Wiley & sons: New York, 1977; Vol. 1.

(51) Demtröder, W. *Laser Spectroscopy*; Springer-Verlag: Berlin, 1981.

(52) Barclay, V. J.; Dateo, C. E.; Hamilton, I. P.; Kendrick, B.; Pack, R. T.; Schwenke, D. W. *J. Chem. Phys.* **1995**, *103*, 3864.

(53) Kendrick, B.; Pack, R. T. *J. Chem. Phys.* **1997**, *106*, 3519.